Quantum theory of a thresholdless laser

I. Protsenko,[1] P. Domokos,[2,*] V. Lefèvre-Seguin,[2] J. Hare,[2] J. M. Raimond,[2] and L. Davidovich[3]

[1]*Lebedev Physics Institute, Leninsky Prospect 53, 117924 Moscow, Russia*
[2]*Laboratoire Kastler-Brossel,[†] Département de Physique de l'Ecole Normale Supérieure, 24 rue Lhomond, 75231 Paris, France*
[3]*Instituto de Fisica, Universidade Federal do Rio de Janeiro, Caixa Postal 68528, 21945-970 Rio de Janeiro, RJ, Brasil*

We develop a quantum theory of a single-mode thresholdless laser. We start from basic Heisenberg–Langevin equations of motion for the field and atomic operators, and obtain an approximate analytical solution to these operator equations. We compare the predictions of this model for the intensity and power spectrum of the field to the results of a Monte Carlo numerical simulation of the original Heisenberg-Langevin equations, and find them in excellent agreement. We also compare these predictions to those of a rate-equation model, which takes into account spontaneous emission. We show that our model gives more reliable results in the bad cavity limit at high intensities. Based upon these results, we propose a simple characterization of the thresholdless behavior. Finally, we apply our model to microsphere Nd-doped lasers at low temperatures, which are promising devices for a well-controlled thresholdless operation. [S1050-2947(99)10502-X]

PACS number(s): 42.55.Ah, 42.55.Sa, 32.80.−t

I. INTRODUCTION

Lasers with small active medium volumes, on the order of hundreds of μm^3, and very low pump energy, oscillating with an average number of photons on the order of 1, have been developed in recent years, motivated by the potential applications in optical communication and information processing. Quantum effects become obviously important in this case, and the semiclassical approach fails to offer a proper description even of the gross overall features of these devices. The very notion of oscillation threshold breaks down, since the output intensity increases smoothly with the pump energy. These devices are thus called thresholdless lasers. Central to this behavior is the fact that, with such a low number of photons, spontaneous emission into the mode plays a very important role. The fraction of spontaneous emission emitted into the mode has indeed been used, for semiconductor lasers, as a measure of the degree of thresholdless behavior.

Thresholdless laser operation was reported for the first time in Ref. [1], for a dye laser with half of the wavelength distance between the cavity mirrors. In this experiment, the threshold pump power was less than the sensitivity limit of the measurement device. Very low oscillation thresholds have been observed since then in several types of lasers, as, for example, in vertical cavity surface-emitting semiconductor lasers (VCSEL's) [2,3], heterostructure diode lasers [4], microdroplets [5], high-Q Fabry-Perot microcavity lasers [6], and microsphere lasers [7].

Theories of low-threshold lasers [8–10] were developed mostly in connection with VCSEL's, which have attracted great attention in the last few years. The threshold of VCSEL's is very low due to two factors: (i) the large value of the field-medium coupling constant, because of the small cavity volume and large amplification coefficient; and (ii) the suppression of spontaneous emission outside of the laser mode, since only a few well-spaced modes are available in the cavity [11,12].

The theory developed in Refs. [8–10] is based on rate equations for the field intensity and carrier density [13], with the addition of terms describing spontaneous emission into the lasing mode and the consequent depletion of the carrier density. A new definition for the laser threshold was proposed in Ref. [10], as the situation in which the number of photons in the lasing mode is equal to 1. Results for VCSEL's were presented in Ref. [11], as a function of the fraction β of spontaneous emission into the laser mode. Smooth transitions through the threshold for $\beta \approx 1$, suppression of relaxation oscillations and linewidth enhancement in the near-to-threshold region were predicted. A semiclassical study of the laser transition, including a contribution from spontaneous emission into the lasing mode, was presented in Ref. [14].

The above-mentioned theoretical models hold if the polarization relaxation rate $\Gamma_\perp$ is larger than the rate of any other process in the laser. However, even in semiconductor lasers where $\Gamma_\perp$ is quite large, $\Gamma_\perp \sim 10^{13}$ Hz [15], the damping rate κ of a vertical cavity may be of the same order of magnitude as $\Gamma_\perp$. For example, for a cavity length $L \sim 1$ μm and a reflection coefficient of the cavity mirrors $R = 0.9$, one has $\kappa \approx \log(R)c/L \approx 10^{13}$ Hz$\approx \Gamma_\perp$, where c is the speed of light.

The same may be true for a microsphere laser. In the experiment reported in Ref. [7], neodymium ions (10^{19} atoms per cm^3) are embedded into a silica microsphere (diameter 50 μm). The effective volume of the field mode is of the order of $500\lambda^3 \approx 500$ μm^3, so that there are about 3×10^9 neodymium ions in the mode volume. Measurements [7] were performed at room temperature and, under this con-

dition, the laser exhibits a well-defined threshold. The pump power at threshold was of the order of 200 nW and laser oscillation was sustained with only 10^5 excited ions at a time. In the semiclassical Lamb model, perfectly valid in this case, the threshold depends linearly on the homogeneous linewidth of the lasing transition. This linewidth is expected to decrease with temperature, from 1500 GHz at 300 K to perhaps as low as 20 MHz at 2 K. The mode linewidth, for a quality factor $Q \sim 2 \times 10^8$, is in the range 2–10 MHz. Thus, at low temperatures, the polarization decay rate (proportional to the inverse of the homogeneous linewidth) and the cavity decay rate (proportional to the inverse of the mode linewidth) should become comparable. Furthermore, under the same conditions, the laser should become thresholdless: oscillation may occur with one photon only in the mode, which precludes using linearization techniques to study the quantum dynamics. A simple model describing the quantum features of this interesting laser situation is therefore in a high demand.

In this paper, we develop a theoretical model for a thresholdless atomic laser, starting from Heisenberg-Langevin operator equations and taking into account the polarization dynamics. We solve the problem both by an approximate analytical technique and by a numerical procedure which takes into account the nonlinear quantum dynamics of the field and atomic variables. The analytical approximation is based on the fact that, in the systems under consideration, the number of active atoms is much larger than the number of photons in the mode, so that the relative fluctuations in the population inversion are much smaller than the relative fluctuations in the number of photons. We use this fact to replace the inversion by a *c* number. However, we do not neglect quantum correlations between the field amplitude operators and the atomic polarization; such an approximation should be indeed very bad below and near the threshold, since the average value of the field amplitude on the time scale of interest is zero, due to phase diffusion [16]. Our approach, validated by a good agreement with the numerical results, leads to smooth analytical expressions for the field intensity, the spectrum, and the linewidth, in regions of parameters where the polarization cannot be adiabatically eliminated and where linearization is forbidden (due to the low values of the average intensity, down to less than one photon in the mode). These expressions remain valid for a wide range of parameters, which may include the low-pumping, low-intensity quantum regime as well as the high-pumping semiclassical limit. The role of the spontaneous emission in the laser cavity can be examined in detail, since spontaneous emission is well described by our quantum operator equations. We are therefore able to follow the transition from the spontaneous-emission-dominated regime to the situation, typical of standard laser operation, in which stimulated emission plays the dominant role. The notion of threshold and thresholdless operation can be put under a new light, allowing us to define a simple and physically transparent criterion for the thresholdless operation.

We will also compare the quantum approach to a simpler rate-equation model, derived from the same Heisenberg-Langevin equations by neglecting the quantum correlations between the atomic inversion and the photon number fluctuations. Similar rate equations, using most often an adia-
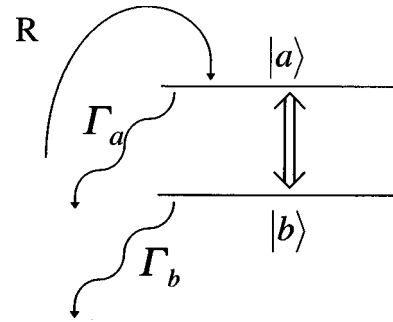

FIG. 1. Relevant level scheme.

batic elimination of the atomic polarization [13], have already been obtained in a large number of papers. The steady-state operating point can be obtained without the adiabatic elimination, and should be valid even in the bad-cavity limit. We will show that the predictions of this rate-equation model are in perfect agreement with ours in the good-cavity limit. However, the rate-equation model deviates significantly from the quantum one and from the standard Lamb theory in the bad-cavity limit at high intensities. This observation casts some doubts on the validity of the rate-equation models in this regime.

The notations used throughout the paper are the same as in Ref. [17]. In Sec. II, we describe the model and the basic Heisenberg-Langevin equations. We establish a very general and exact relation between the steady-state average values of the population inversion and the intensity. We also introduce the solutions of the standard semiclassical Lamb model as useful scaling parameters. In Sec. III, we derive, from Heisenberg-Langevin equations, rate equations for the photon number and atomic populations, taking into account spontaneous emission terms. The approximate analytic quantum model is introduced in Sec. IV. We check that, under proper conditions, treating the inversion as a *c*-number does not affect the commutation relations involving the other operators. The solutions for the average intensity and the spectrum are then derived. We also obtain the spontaneous emission rate into the laser mode. The numerical method is developed in Sec. V. We discuss the relation between the results of the different models in Sec. VI, where a precise characterization of the thresholdless behavior, valid beyond the rate-equation limit, is proposed. In this section we discuss the quantitative predictions of the models using parameters pertaining to the microsphere neodymium lasers at low temperature. Finally, our conclusions are summarized in Sec. VII.

II. QUANTUM-MECHANICAL SINGLE-MODE LASER MODEL

We describe the active medium by two-level atoms (upper level *a*, lower level *b*), resonant with a single-cavity mode damped at a rate κ. Levels *a* and *b* decay to lower levels, with decay constants Γ_a and Γ_b respectively, as shown in Fig. 1. The relaxation rate Γ_a is most often much smaller than Γ_b. When this is not the case, laser oscillation can hardly be sustained. The atoms are uniformly coupled to the field with a coupling constant *g*, equal to half the Rabi precession frequency in a single photon field. Inhomogeneous

broadening and mode competition are neglected. This is a severe approximation for most solid-state laser systems, such as neodymium doped microspheres where the emission linewidth is larger than the mode spacing. However, in many cases, the homogeneous width of the transition, Γ_{ab}, is smaller than or comparable to the cavity mode spacing. In such cases, there is no mode competition, and a given class of atoms in the inhomogeneously broadened spectrum emits only in a single mode of the cavity. The detunings of the atoms inside the homogeneous linewidth may be accounted for by using an effective atom-field coupling, thus validating our model. We assume also that the number of active atoms is large enough so that the pumping process can be considered as Poissonian and can be simply described by a pumping rate R in the equation of motion for the population of level a [18] (this is consistent with the experimental situations regarding heavily doped microspheres which have a large number of accessible nonexcited ions and a very low number of excited ions at a time).

We base our approach on the following Heisenberg-Langevin equations, written in the interaction picture. They can be derived from first principles as shown in detail in Ref. [17]:

$$\dot{a}(t) = gM(t) - \kappa/2\, a(t) + F_\kappa(t), \quad (1a)$$

$$\dot{M}(t) = g[N_a(t) - N_b(t)]a(t) - \Gamma_{ab}M(t) + F_M(t), \quad (1b)$$

$$\dot{N}_a(t) = R - g[a^\dagger(t)M(t) + M^\dagger(t)a(t)] - \Gamma_a N_a(t) + F_a(t), \quad (1c)$$

$$\dot{N}_b(t) = g[a^\dagger(t)M(t) + M^\dagger(t)a(t)] - \Gamma_b N_b(t) + F_b(t), \quad (1d)$$

where a and $a^\dagger$ are the boson operators of the field mode, M is the collective atomic polarization, and N_a and N_b are the populations in levels a and b, respectively. The noise features are incorporated into the F reservoir operators. They obey the usual Langevin correlations

$$\langle F_i(t) \rangle = 0,$$
$$\langle F_i(t)F_j(t') \rangle = 2D_{ij}\delta(t-t'), \quad (2)$$

where the nonvanishing diffusion coefficients at zero temperature are

$$2D_{\kappa\kappa^\dagger} = \kappa,$$

$$2D_{M^\dagger M} = (2\Gamma_{ab} - \Gamma_a)\langle N_a(t) \rangle + R,$$

$$2D_{MM^\dagger} = (2\Gamma_{ab} - \Gamma_b)\langle N_b(t) \rangle, \quad (3)$$

$$2D_{aa} = \Gamma_a\langle N_a(t) \rangle + R, \quad 2D_{bb} = \Gamma_b\langle N_b(t) \rangle,$$

$$2D_{bM} = \Gamma_b\langle M(t) \rangle, \quad 2D_{Ma} = \Gamma_a\langle M(t) \rangle.$$

No general solution for this model has been found so far. In the region high above threshold, one may linearize these equations (or a c-number version of them [19]) around the steady state and calculate the spectra of fluctuations. Well below threshold, one may consider the populations of the

lasing levels as c-number constants, given by their zero-field values, the so-called unsaturated values [20]. However, none of these procedures can be applied to thresholdless lasers. In this paper we will discuss two different approaches and compare them to the standard semiclassical Lamb model [21]. We will first derive rate equations for the quantum averages, taking into account properly the spontaneous emission in the cavity mode. We then develop an approximate quantum model which leads to analytical operator solutions, allowing us to derive explicit forms for the output intensity and the power spectrum. The solutions of these models are compared with numerical results, obtained by a method detailed in Sec. V.

Before analyzing these models, we briefly recall the Lamb semiclassical model. It will be used, throughout the paper, as a source of useful scaling parameters for our solutions. It can be recovered from Eq. (1) by considering all the operators as mere c-numbers, and suppressing the noise terms. The steady-state solution can be easily obtained without any further approximation. The oscillation threshold is given by

$$R_{\text{th}} = \frac{\kappa\Gamma_a\Gamma_{ab}}{2g^2}. \quad (4)$$

If $R < R_{\text{th}}$, the semiclassical steady-state intensity is equal to zero and the steady-state population inversion is given by R/Γ_a. For $R \gg R_{\text{th}}$, the semiclassical steady-state mean photon number is given by

$$I_0 = I_{\text{sat}}(R/R_{\text{th}} - 1), \quad (5)$$

where the "saturation intensity" I_{sat} is

$$I_{\text{sat}} = \frac{\Gamma_a\Gamma_{ab}\Gamma_b}{2g^2(\Gamma_a + \Gamma_b)} = \frac{R_{\text{th}}}{\kappa}\frac{1}{1 + \Gamma_a/\Gamma_b}. \quad (6)$$

Above threshold, the population inversion is independent of the pumping rate (this is the "population clamping" effect, characteristic of homogeneously broadened lasers) and given by

$$\Delta_0 = \frac{\kappa\Gamma_{ab}}{2g^2}. \quad (7)$$

The Lamb model is expected to coincide with the solution of our model when the laser has a well-defined threshold and operates far above it.

We now derive, from the Heisenberg-Langevin equations, an exact relation between the population inversion and the intensity which will be very useful in the following. Let us first introduce the photon number operator $n = a^\dagger a$ and an operator Λ defined as

$$\Lambda = a^\dagger M + M^\dagger a. \quad (8)$$

The Heisenberg-Langevin equations can be easily rewritten in terms of n and Λ as

$$\dot{n} = -\kappa n + g\Lambda + a^\dagger F_\kappa + F_\kappa^\dagger a, \quad (9a)$$

$$\dot{\Lambda} = 2ga^\dagger(N_a - N_b)a - (\Gamma_{ab} + \kappa/2)\Lambda + 2gM^+M$$
$$+ a^\dagger F_M + F_M^\dagger a + F_\kappa^\dagger M + M^\dagger F_\kappa, \tag{9b}$$

$$\dot{N}_a = R - g\Lambda - \Gamma_a N_a + F_a, \tag{9c}$$

$$\dot{N}_b = g\Lambda - \Gamma_b N_b + F_b. \tag{9d}$$

The quantum average values of these operator equations are obviously written

$$\langle \dot{n} \rangle = -\kappa\langle n \rangle + g\langle \Lambda \rangle, \tag{10a}$$

$$\langle \dot{\Lambda} \rangle = -(\Gamma_{ab} + \kappa/2)\langle \Lambda \rangle + 2g\langle N_a \rangle + 2g\langle (N_a - N_b)n \rangle. \tag{10b}$$

$$\langle \dot{N}_a \rangle = R - \Gamma_a\langle N_a \rangle - g\langle \Lambda \rangle, \tag{10c}$$

$$\langle \dot{N}_b \rangle = -\Gamma_b\langle N_b \rangle + g\langle \Lambda \rangle. \tag{10d}$$

To obtain Eq. (10b), we made use of the relation $\langle M^\dagger M \rangle = \langle N_a \rangle$ [see Eq. (6.18) in Ref. [17]] and the commutation of $a^\dagger$ with $N_a - N_b$. From Eqs. (10), one obtains a useful relation between the average population inversion $\Delta \equiv \langle N_a - N_b \rangle$ and the average intensity $I \equiv \langle n \rangle$ in the steady state. From Eq. (10a), we have $I = (g/\kappa)\langle \Lambda \rangle$. Using this expression in Eqs. (10c) and (10d) for the steady-state populations, we obtain

$$\Gamma_a\langle N_a \rangle = R - \kappa I, \quad \Gamma_b\langle N_b \rangle = \kappa I. \tag{11}$$

It follows that the steady-state population inversion is connected to the mean intensity by

$$\frac{\Delta - \Delta_0}{\Delta_0} = \frac{I_0 - I}{I_{\text{sat}}}. \tag{12}$$

We emphasize that Eq. (12) is a universal and exact balance equation which must hold in all single-mode, two-level, laser models at zero temperature. Clearly, the semiclassical results for the population inversion and for the intensity obey Eq. (12) since both sides are zero in this case. With this relation, we will easily be able to obtain the population inversion from the average intensity. This will make the algebra noticeably more simple in the following.

III. QUANTUM RATE EQUATIONS

The exact equations (10) for the quantum average values have no explicit solution, even for the steady state. This set of equations is indeed incomplete, since an equation for $\langle (N_a - N_b)n \rangle$, involving higher-order moments, is necessary. In this section we will discuss a simple rate-equation model obtained by neglecting the correlations between the population inversion and the photon number, and letting $\langle (N_a - N_b)n \rangle \approx \langle N_a - N_b \rangle\langle n \rangle$. Thus from the basic Heisenberg-Langevin equations and at the expense of a single approximation, the validity of which will be discussed later, we obtain a closed set of rate equations for the average values

$$\langle \dot{n} \rangle = -\kappa\langle n \rangle + g\langle \Lambda \rangle, \tag{13a}$$

$$\langle \dot{\Lambda} \rangle = 2g\langle (N_a - N_b) \rangle\langle n \rangle - (\Gamma_{ab} + \kappa/2)\langle \Lambda \rangle + 2g\langle N_a \rangle, \tag{13b}$$

$$\langle \dot{N}_a \rangle = R - g\langle \Lambda \rangle - \Gamma_a\langle N_a \rangle, \tag{13c}$$

$$\langle \dot{N}_b \rangle = g\langle \Lambda \rangle - \Gamma_b\langle N_b \rangle. \tag{13d}$$

Note that the relaxation rate of $\langle \Lambda \rangle$ is $(\Gamma_{ab} + \kappa/2)$, combining the polarization and cavity damping rates. This set of rate equations, which does not seem to have been derived before, is obtained without any assumption regarding the relative magnitude of the decay constants. One thus might expect this model to be valid either in the good-cavity limit ($\Gamma_{ab} \gg \kappa$) or in the bad-cavity one ($\Gamma_{ab} \ll \kappa$). We will show later on, however, that these equations do not provide a good approximation to the steady-state solution high above threshold, unless $\kappa \ll \Gamma_{ab}$ which corresponds to the good-cavity limit.

A simpler set of equations may be obtained when the relaxation rate $\Gamma_{ab} + \kappa/2$ is much greater than the atom-field coupling g, as well as κ, Γ_a, and Γ_b. This condition, which holds in the good-cavity limit, is satisfied by several kinds of lasers [17]. One is then allowed to eliminate Λ adiabatically. One should note that this adiabatic elimination is legitimate in principle only for the equations involving the averages of operators, since the operator equations themselves include fast-varying fluctuating forces. After this elimination, one obtains a closed set of equations:

$$\langle \dot{n} \rangle = -\kappa\langle n \rangle + W\langle (N_a - N_b) \rangle\langle n \rangle + W\langle N_a \rangle, \tag{14a}$$

$$\langle \dot{N}_a \rangle = R - \Gamma_a\langle N_a \rangle - W\langle (N_a - N_b) \rangle\langle n \rangle - W\langle N_a \rangle, \tag{14b}$$

$$\langle \dot{N}_b \rangle = -\Gamma_b\langle N_b \rangle + W\langle (N_a - N_b) \rangle\langle n \rangle + W\langle N_a \rangle, \tag{14c}$$

where

$$W = \frac{2g^2}{\Gamma_{ab} + \kappa/2}. \tag{15}$$

These rate equations obviously contain spontaneous emission contributions [the last terms on the right-hand side of Eqs. (14)] neglected in the semiclassical treatment [22]. The spontaneous emission rate in the lasing mode is W. As we will see in the following, this rate plays a central role in the thresholdless laser condition.

Since Eqs. (14) are valid in the good-cavity limit ($\kappa \ll \Gamma_{ab}$), the κ terms in the spontaneous emission rate W could have been neglected. However, in the following, we will rather be interested in the steady-state solutions of Eqs. (13), which should also be valid in the bad-cavity limit. The cavity damping contribution to W will therefore be retained.

A widely used benchmark for the thresholdless behavior of a laser is the parameter β defined as the fraction of the spontaneous emission rate corresponding to emission into the lasing mode. Under certain conditions, semiconductor lasers become thresholdless when $\beta \sim 1$ (see, for instance, the discussion in Ref. [10]). In order to estimate the feasibility of a thresholdless laser, one can compare W to the total spontaneous emission rate in bulk space Γ_a^{sp}, since $\beta \sim 1$ is expected to occur when $W \gg \Gamma_a^{\text{sp}}$. Taking the basic expressions

of Γ_a^{sp} and g for a dipole embedded in a bulk medium with an index of refraction N [23], one obtains a simple relation between W and Γ_a^{sp} similar to the Purcell factor discussed in Ref. [24],

$$\frac{W}{\Gamma_a^{sp}} = \frac{3}{4\pi^2} \frac{\omega}{\Gamma_{ab}+\kappa/2} \frac{(\lambda/N)^3}{V} \;. \tag{16}$$

where ω and λ are the angular frequency and wavelength of the dipole transition, and V is the cavity mode volume. This expression shows that it is possible to achieve $W \gg \Gamma_a^{sp}$ for a narrow enough transition line resonant with a high-Q microcavity mode.

The connection between β and W/Γ_a^{sp} depends on the type of cavity one considers. For open cavities, spontaneous emission in all the side modes will be only weakly affected, and it is legitimate to write the fraction of the spontaneous emission in the laser cavity mode as

$$\beta = \frac{W}{\Gamma_a^{sp}+W} \;. \tag{17}$$

This equation will not hold for a closed microcavity, for which the total decay rate by spontaneous emission from level a will depend on its specific geometry.

Of course, if processes other than spontaneous emission contribute to the decay of level a with a rate Γ_a^*, one should rather consider the ratio W/Γ_a with $\Gamma_a = \Gamma_a^{sp}+\Gamma_a^*$. The condition $\beta \sim 1$ does not necessarily lead then to thresholdless behavior, and a stronger condition is needed, as will be shown in Sec. VI B.

The steady-state solution of the complete equations (13) can be obtained exactly. As we mentioned before, the adiabatic elimination (setting the time derivative of the polarization to zero) is not needed for the steady state, since all time derivatives are zero. To provide an easy comparison with the semiclassical Lamb model, here we use the scaled variables $i_{re} = I/I_{sat}$ and $r = R/R_{th}$. For the intensity we obtain a second-order algebraic equation

$$i_{re}^2 + i_{re}(1-r+b) - b'r = 0, \tag{18}$$

where

$$b = \frac{\kappa/2}{\Gamma_{ab}} + \frac{2g^2}{\Gamma_a \Gamma_{ab}}, \quad b' = \frac{1}{I_{sat}} \;. \tag{19}$$

The solution of Eq. (18) is given by

$$i_{re\pm} = \tfrac{1}{2}(r-1-b) \pm \tfrac{1}{2}\sqrt{(r-1-b)^2 + 4b'r}. \tag{20}$$

Only the root i_+ behaves correctly at zero pumping, predicting a zero intensity. It is the only acceptable solution. A similar second-order equation could have been derived for the population inversion. However, it suffices to calculate the intensity and then use Eq. (12) to determine Δ.

This rate-equation model handles only average values of the intensity or of the population inversion. It is not quite suited to compute higher-order correlation functions or the field spectrum. Qualitative values for the linewidth may be derived from the eigenfrequencies of the dynamical system

(14), linearized around the steady-state operating point. The discussion of the rate-equation model predictions is deferred to Sec. VI C.

The spectrum or the correlations can be adequately described only by a quantum model, where the operator nature of the quantities of interest would be retained. The power spectrum, for instance, could be calculated directly from its definition, i.e., the two-time correlation function of the field operators. Such a model also includes the Langevin noises that were bypassed in the rate-equation approach. In Sec. IV we proceed to establish such a quantum model.

IV. APPROXIMATE QUANTUM MODEL

A. Main assumption

The basic assumption in the following analytical treatment is that the population inversion is large enough so that its fluctuations can be neglected. This assumption is reasonable for many laser systems, especially for microlasers where the number of atoms taking part in the interaction is typically much larger than the generated photon number. We will verify later, by comparing the corresponding analytical solutions with numerical results, that this approximation is indeed very good over a wide range of parameters.

The crucial step in applying this assumption is the replacement of the operator representing the population inversion in Eq. (1b) by its mean value. Since we are only interested in the mean values of the atomic population operators, we may replace Eqs. (1c) and (1d) with Eqs. (10c) and (10d). The new set of equations to be solved is then

$$\dot{a}(t) = gM(t) - \frac{\kappa}{2}a(t) + F_\kappa(t), \tag{21a}$$

$$\dot{M}(t) = g\langle N_a(t) - N_b(t)\rangle a(t) - \Gamma_{ab}M(t) + F_M(t), \tag{21b}$$

$$\langle \dot{N}_a(t)\rangle = R - g\langle a^\dagger(t)M(t) + M^\dagger(t)a(t)\rangle - \Gamma_a\langle N_a(t)\rangle, \tag{21c}$$

$$\langle \dot{N}_b(t)\rangle = g\langle a^\dagger(t)M(t) + M^\dagger(t)a(t)\rangle - \Gamma_b\langle N_b(t)\rangle. \tag{21d}$$

Since, for the systems under consideration, the intensities involved will be very low, down to a few photons, we are not allowed to linearize these equations around the steady-state values. On the other hand, we will be interested in the behavior of the steady state, and Eqs. (21) should therefore be considered after the transients die out and all average quantities become constants. The essential parts of the Heisenberg-Langevin equations left to be solved are

$$\dot{a}(t) = gM(t) - \frac{\kappa}{2}a(t) + F_\kappa(t), \tag{22a}$$

$$\dot{M}(t) = g\Delta a(t) - \Gamma_{ab}M(t) + F_M(t), \tag{22b}$$

which comprise coupled linear differential equations containing the population inversion as a c-number constant parameter Δ. The actual value of Δ can be determined from Eq. (12) in a self-consistent way. The inversion being treated

as a number, we obviously neglect, as in the rate-equation model, the correlations between the intensity and the population inversion. However, we keep the whole field-polarization correlations. Moreover, the dynamics of the population inversion obviously include nonvanishing second-order correlations of the Langevin noises which were neglected previously.

B. Operator algebra and validity conditions

When replacing one operator by a *c*-number in the original Heisenberg-Langevin equations, one might fear that the operator solutions of the equations would no longer obey the standard commutation rules. We have to check this point before proceeding to solve the model. The population inversion being only a source term in the polarization dynamics, we have to check the polarization commutation rule, which is written [17]

$$[M^\dagger(t), M(t)] = N_a - N_b. \tag{23}$$

We have here, at variance,

$$[M^\dagger(t), M(t)] \approx \Delta = \text{const.} \tag{24}$$

Therefore, our approximation implies that the atomic polarization operator behaves like a bosonic operator

$$M(t) = \begin{cases} \sqrt{|\Delta|}\, b^\dagger(t) & \text{if } \Delta \geq 0 \\ \sqrt{|\Delta|}\, b(t) & \text{if } \Delta < 0, \end{cases} \tag{25}$$

where $[b(t), b^\dagger(t)] = 1$. Consequently, the associated Langevin noise operators should obey the commutation relation

$$\langle [F_M^\dagger(t), F_M(t')] \rangle = 2\Gamma_{ab}\Delta\, \delta(t - t'), \tag{26}$$

just as the field noise F_κ does. However, it follows from Eq. (3) that

$$\langle [F_M^\dagger(t), F_M(t')] \rangle$$
$$= (2\Gamma_{ab}\Delta + R - \Gamma_a\langle N_a\rangle + \Gamma_b\langle N_b\rangle)\, \delta(t - t'). \tag{27}$$

The necessary condition for approximation (25) to hold is therefore that the difference between the expressions on the right-hand side of Eqs. (26) and (27) becomes negligible. This implies that

$$2\Gamma_{ab}\Delta \gg R - \Gamma_a\langle N_a\rangle + \Gamma_b\langle N_b\rangle. \tag{28}$$

On the other hand, in the steady state, it follows from Eq. (11) that $R - \Gamma_a\langle N_a\rangle = \Gamma_b\langle N_b\rangle = \kappa I$. Therefore, as a necessary condition for the consistency of approximation (25), we obtain

$$\Delta \gg (\kappa/\Gamma_{ab}) I. \tag{29}$$

For large enough intensities, for lasers operating far above threshold, this condition is bound to be violated. One might thus expect that our quantum model is valid only in a limited region below and near threshold, especially when $\Gamma_{ab} \lesssim \kappa$. We will see in fact that it gives sound results even in the high-intensity limit.

Since condition (29) plays a central role in our model, it is important to write it in a physically more transparent way. Introducing Δ_0, condition (29) can be written as

$$\Gamma_{ab} \gg \frac{\kappa}{\Delta_0} I \frac{\Delta_0}{\Delta}. \tag{30}$$

Noting that $\kappa/\Delta_0 = 2g^2/\Gamma_{ab}$ and that, above threshold, Δ_0/Δ is expected to be on the order of 1, this condition can finally be written

$$\Gamma_{ab} \gg g\sqrt{I}. \tag{31}$$

This condition has a very simple physical interpretation. $g\sqrt{I}$ is the Rabi frequency of an atom in the cavity field. The validity condition of the model, in the region high above threshold, is thus that the polarization relaxation dominates the Rabi precession in the laser field. This is a weak-coupling condition (the weak-coupling condition for a single atom in the empty cavity is written $\Gamma_{ab} \gg g$).

Equation (29) leads to an approximate expression for the diffusion coefficient $D_{M^\dagger M}$. Indeed, since for positive inversion $\langle N_a\rangle \geq \Delta > 0$, Eq. (29) implies that $2\Gamma_{ab}\langle N_a\rangle \gg \kappa I = R - \Gamma_a\langle N_a\rangle$. Therefore, one should take

$$2D_{M^\dagger M} \approx 2\Gamma_{ab}\langle N_a\rangle \tag{32}$$

in all subsequent calculations in order not to obtain inconsistent results. In fact, only this diffusion coefficient is necessary for the following treatment, since the quantities of interest (intensity and power spectrum) will be defined in terms of normal-ordered products of field operators. Therefore, one does not need to approximate $D_{MM^\dagger}$.

C. Dynamical behavior: stability conditions

Before discussing the steady-state solutions for the intensity and the power spectrum, we analyze the stability of the steady state by examining the eigenvalues of the homogeneous part of Eq. (22), that is,

$$\dot{a}(t) = gM(t) - \frac{\kappa}{2}a(t), \tag{33a}$$

$$\dot{M}(t) = g\Delta a(t) - \Gamma_{ab}M(t). \tag{33b}$$

The corresponding solutions will describe the transient behavior of the field and polarization operators, which is related to the relaxation of the fluctuations in the field amplitude and in the atomic polarization. Indeed, for the steady state, one should have $\langle a(t)\rangle = \langle M(t)\rangle = 0$ due to phase diffusion. However, an arbitrary fluctuation in the system state should render these average values different from zero. Their subsequent behavior can be obtained from the time-dependent solutions of Eq. (33). The associated eigenmodes will be given by

$$a(t) = a(0)e^{\lambda t}, \quad M(t) = M(0)e^{\lambda t}. \tag{34}$$

Replacing Eq. (34) in Eqs. (33), we obtain

$$\tilde{D}(\lambda) = \left(\lambda + \frac{\kappa}{2}\right)(\lambda + \Gamma_{ab}) - g^2\Delta = 0 \tag{35}$$

with roots given by

$$\lambda_{\pm} = -\left[\frac{1}{2}\left(\frac{\kappa}{2}+\Gamma_{ab}\right) \pm \frac{1}{2}\sqrt{\left(\frac{\kappa}{2}-\Gamma_{ab}\right)^2 + 4g^2\Delta}\right], \quad (36)$$

so that $\lambda_{\pm}$ is real. There are therefore no relaxation oscillations. One should note that the absence of relaxation oscillations, predicted by our analysis, is a consequence of neglecting the population fluctuations. The numerical simulations presented in Sec. V, for which this assumption is not made, will confirm our analytical results, in the sense that relaxation oscillations do show up but with a very small amplitude, much smaller than those predicted by semiclassical models. When $g^2\Delta \rightarrow 0$, these two solutions yield $\lambda_+ \rightarrow -\kappa/2$ and $\lambda_- \rightarrow -\Gamma_{ab}$, so that in this case we may call λ_+ and λ_- the "field-dominated" and "polarization-dominated" modes, respectively.

We must have $\lambda_{\pm} < 0$ in order to avoid runaway solutions. Rewriting Eq. (36) as

$$\lambda_{\pm} = -\frac{1}{2}\left(\frac{\kappa}{2}+\Gamma_{ab}\right)\left[1 \pm \sqrt{1 - \frac{2\kappa\Gamma_{ab}}{(\kappa/2+\Gamma_{ab})^2}\left(1-\frac{\Delta}{\Delta_0}\right)}\right], \quad (37)$$

where Δ_0 is given by Eq. (7), we can see that $\lambda_{\pm} < 0$ if and only if

$$\Delta < \Delta_0. \quad (38)$$

This condition implies that the population inversion must always be smaller than its semiclassical threshold value, which has a simple physical interpretation (cf. the equivalent discussion in Ref. [10]): the semiclassical threshold is obtained by equating the optical gain to the cavity losses; however, the presence of spontaneous emission into the lasing mode implies that the optical gain must always be smaller than the cavity losses, and therefore the inversion must be smaller than the corresponding semiclassical threshold value. It follows immediately from this condition, and from Eq. (12), that $I - I_0 > 0$, which can also be interpreted as a consequence of the fact that I_0 does not include the spontaneous emission contribution.

D. Steady-state solutions

1. Fourier transforms of operators

We look now for the solutions of Eqs. (22) after the transients have died out. Since the system involves Langevin noises, the time derivatives do not vanish, even in the steady state. The operator solutions of the system may thus be obtained by the Fourier transform method (the complete solution, including the initial conditions, may be obtained by the Laplace transform method). We define

$$O(t) = \frac{1}{\sqrt{2\pi}}\int_{-\infty}^{\infty} d\omega\, e^{-i\omega t} O(\omega),$$

$$O^{\dagger}(t) = \frac{1}{\sqrt{2\pi}}\int_{-\infty}^{\infty} d\omega\, e^{i\omega t} O^{\dagger}(\omega),$$

so that the noise correlations for the Fourier-transformed Langevin operators become

$$\langle F_i(\omega)F_j(\omega')\rangle = 2D_{ij}\delta(\omega+\omega'),$$

$$\langle F_i^{\dagger}(\omega)F_j(\omega')\rangle = 2D_{ij}\delta(\omega-\omega').$$

The Fourier transformation applied to Eqs. (22) yields

$$(\kappa/2 - i\omega)a(\omega) - gM(\omega) = F_{\kappa}(\omega), \quad (39a)$$

$$-g\Delta a(\omega) + (\Gamma_{ab} - i\omega)M(\omega) = F_M(\omega), \quad (39b)$$

so that

$$a(\omega) = \frac{1}{D(\omega)}[(\Gamma_{ab}-i\omega)F_{\kappa}(\omega) + gF_M(\omega)], \quad (40a)$$

$$M(\omega) = \frac{1}{D(\omega)}[g\Delta F_{\kappa}(\omega) + (\kappa/2-i\omega)F_M(\omega)], \quad (40b)$$

where

$$D(\omega) = (\kappa/2-i\omega)(\Gamma_{ab}-i\omega) - g^2\Delta$$
$$= g^2(\Delta_0-\Delta) - \omega^2 - i\omega(\kappa/2+\Gamma_{ab}). \quad (41)$$

We obviously have $D(\omega) = \tilde{D}(-i\omega)$. Therefore, the roots of $D(\omega)$ may be written as $\omega_{\pm} = i\lambda_{\pm}$, where $\lambda_{\pm}$ are the damping rates of the transient solutions, given by Eq. (36). In terms of these roots, we may write

$$D(\omega) = (\omega - i\lambda_+)(\omega - i\lambda_-), \quad (42)$$

where, as seen before, $\lambda_{\pm}$ are real. These results will now be used to calculate the steady-state values for the intensity and the population inversion, as well as the power spectrum of the laser field.

2. Intensity and population inversion

From Eq. (40a), and using the fact that $\langle F_{\kappa}^{\dagger}(\omega)F_{\kappa}(\omega')\rangle$ as well as the cross-correlations between the field and the atomic polarization Langevin forces vanish at zero temperature, we obtain

$$\langle a^{\dagger}(\omega)a(\omega')\rangle = S(\omega)\delta(\omega-\omega'), \quad (43)$$

where

$$S(\omega) = \frac{2g^2 D_{M^{\dagger}M}}{|D(\omega)|^2} \quad (44)$$

is the power spectrum of the laser field.

The detailed analysis of the power spectrum will be deferred to Sec. IV D 3. We first calculate the total intensity, given by the integral of the power spectrum over the frequency:

$$\langle a^{\dagger}(t)a(t)\rangle = \frac{1}{2\pi}\int\int d\omega\, d\omega'\, e^{i\omega t}e^{-i\omega' t}\langle a^{\dagger}(\omega)a(\omega')\rangle$$

$$= 2g^2 D_{M^{\dagger}M}\frac{1}{2\pi}\int \frac{d\omega}{|D(\omega)|^2}. \quad (45)$$

The integral in the above equation is evaluated in the Appendix:

$$\frac{1}{2\pi}\int \frac{d\omega}{|D(\omega)|^2} = \frac{1}{2g^2(\Delta_0-\Delta)(\kappa/2+\Gamma_{ab})}. \quad (46)$$

Replacing this result into Eq. (45) and using the expression for $D_{M^\dagger M}$ given by Eq. (32), we obtain

$$I = \frac{\Gamma_{ab}\langle N_a\rangle}{(\Delta_0-\Delta)(\kappa/2+\Gamma_{ab})}. \quad (47)$$

In the steady state, we have from Eq. (11) that $R-\Gamma_a\langle N_a\rangle = \Gamma_b\langle N_b\rangle$, so that

$$\langle N_a\rangle = \frac{R+\Gamma_b\Delta}{\Gamma_a+\Gamma_b}. \quad (48)$$

Inserting this result into Eq. (47), we obtain, together with Eq. (12), a closed set of equations which allow the determination of the steady-state values of the mean intensity and the population inversion:

$$I = \frac{\Gamma_{ab}(R+\Gamma_b\Delta)}{(\Gamma_a+\Gamma_b)(\Gamma_{ab}+\kappa/2)(\Delta_0-\Delta)}, \quad (49a)$$

$$\frac{I-I_0}{I_{\text{sat}}} = \frac{\Delta_0-\Delta}{\Delta_0}. \quad (49b)$$

Equations (49) lead to second-order algebraic equations for both the intensity and the population inversion, extremely similar to the ones derived for the rate-equation model [Eq. (18)]. In terms of the scaled variables $i_{\text{qm}}=I/I_{\text{sat}}$ and $r = R/R_{\text{th}}$, for the intensity we obtain

$$i_{\text{qm}}^2+i_{\text{qm}}(1-r+c)-cr(1+\Gamma_a/\Gamma_b)=0, \quad (50)$$

where

$$c = \frac{1}{I_{\text{sat}}(1+\kappa/2\Gamma_{ab})(1+\Gamma_a/\Gamma_b)} = \frac{2g^2}{\Gamma_a(\Gamma_{ab}+\kappa/2)} = \frac{W}{\Gamma_a}. \quad (51)$$

Note that the parameter c has a very transparent physical interpretation. It is the ratio of the spontaneous emission rate in the mode to the total relaxation rate of level a, and it describes the efficiency of radiation in the cavity mode. One thus expects that thresholdless operation occurs when c is large enough.

The solution of Eq. (50) is given by

$$i_{\text{qm}\pm} = \tfrac{1}{2}(r-1-c)\pm\tfrac{1}{2}\sqrt{(r-1-c)^2+4cr(1+\Gamma_a/\Gamma_b)}. \quad (52)$$

Only the $i_{\text{qm}+}$ solution leads to zero intensity for zero pumping, and we therefore have

$$i_{\text{qm}} = \tfrac{1}{2}(r-1-c)+\tfrac{1}{2}\sqrt{(r-1-c)^2+4cr(1+\Gamma_a/\Gamma_b)}. \quad (53)$$

The linear relation Eq. (49b) can be used to determine Δ from the intensity.

3. *Spontaneous emission rate into the mode*

The spontaneous emission rate into the laser mode is an essential quantity to describe lasers operating close to the thresholdless regime. We have shown in Sec. III that the quantum rate equations naturally incorporate spontaneous emission [see Eqs. (14)], also calculated in Ref. [25]. It is important to check that this more complete quantum model gives the same spontaneous emission rate in the very weak pumping regime, well below the semiclassical threshold, where the only feeding of photons into the mode is due to spontaneous emission. In the steady state, the photons spontaneously emitted in the cavity mode balance the cavity losses. For very small pumping rates R and intensities I, one should have

$$\kappa I = \frac{W}{W+\Gamma_a}R, \quad (54)$$

where W denotes, as above, the rate of spontaneous emission into the single cavity mode. From result (51), it follows that W has the same expression as in the rate-equation model:

$$W = \frac{2g^2}{\Gamma_{ab}+\kappa/2}. \quad (55)$$

The quantum model thus properly accounts for spontaneous emission in the cavity mode.

E. Power spectrum

As we have seen in Sec. IV D, the power spectrum of the laser field is given by Eq. (44). It may be represented in the normalized form

$$\frac{S(\omega)}{2\pi I} = \frac{1}{\pi}\frac{|\lambda_+\lambda_-|}{|\lambda_-|-|\lambda_+|}\left[\frac{1}{\omega^2+\lambda_+^2}-\frac{1}{\omega^2+\lambda_-^2}\right], \quad (56)$$

which is the difference between two Lorentzians with linewidths (full width at half maximum) $2|\lambda_+|$ and $2|\lambda_-|$. These linewidths correspond to the decay rates of the transients and can be immediately obtained from Eq. (37). They are given in terms of the steady-state intensity by

$$\lambda_\pm = -\frac{1}{2}\left(\frac{\kappa}{2}+\Gamma_{ab}\right)\left[1\pm\sqrt{1-\frac{2\kappa\Gamma_{ab}}{(\kappa/2+\Gamma_{ab})^2}(i_{\text{qm}}-i_0)}\right], \quad (57)$$

where $i_0=I_0/I_{\text{sat}}$ is the normalized intensity in the Lamb model.

Spectrum (56) has always a single maximum at $\omega=0$. This behavior reflects the absence of relaxation oscillations in the laser [26] since $\lambda_\pm$ are purely real. Of course, these results have been obtained in the interaction picture where the free evolution of the field is subtracted. The actual spectrum is centered at the atomic transition frequency.

Expression (56) can be simplified if $2\kappa\Gamma_{ab}(i_{\text{qm}}-i_0)/[(\kappa/2)+\Gamma_{ab}]^2\ll1$. This will be the case if $i_{\text{qm}}-i_0\ll1$, which should be valid in the semiclassical limit. This expansion will still hold, however, if $i_{\text{qm}}-i_0\sim1$, provided

that κ and Γ_{ab} differ by at least one order of magnitude. Then, expanding the square root and keeping only the leading terms, we obtain

$$2|\lambda_+| \cong \kappa + 2\Gamma_{ab}, \tag{58}$$

$$2|\lambda_-| \cong \frac{\kappa\Gamma_{ab}}{(\kappa/2+\Gamma_{ab})}(i_{qm}-i_0). \tag{59}$$

In this regime, we have $|\lambda_+| \gg |\lambda_-|$, and the spectrum can be well approximated by one Lorentzian with linewidth $|\lambda_-|$. In this limit, one may associate the narrower Lorentzian with phase fluctuations (note that λ_- is the polarization dominated eigenvalue of the stability analysis of Sec. IV C), while the other has its origin in photon number fluctuations (λ_+ being the field-dominated eigenvalue). This will be the case in the semiclassical limit, in which one usually neglects the contribution of photon number fluctuations to the power spectrum.

On the other hand, if the cavity field damping rate and the homogeneous linewidth of the laser transition are comparable, and if the laser operates close to the semiclassical threshold, so that the term proportional to $i_{qm}-i_0$ inside the square root is not necessarily small, the two Lorentzians yield an anomalous spectral profile. Here, outside the semiclassical limit, one cannot distinguish the contributions from photon number fluctuations and phase diffusion.

V. NUMERICAL MODEL

In order to discuss the validity of the two models presented above, we have derived a numerical solution of the basic Langevin equations. The direct numerical simulation of operator equations is rather impractical. In this section, we develop a numerical method that requires much less computational effort and yet provides equivalent results as long as one is interested in at most second-order correlation functions of the operators.

A. Principles

As it is well known, the operator variables of a quantum-mechanical system may be replaced by c-number variables if a specific operator ordering is defined. In this c-number description, the quantum-mechanical average of an arbitrary physical quantity is represented by a phase-space integral. Our basic idea is to apply the Monte Carlo method to approximate the phase-space integral associated with the required average.

Since there is no product of noncommuting operators in the Heisenberg-Langevin equations, the operator variables $\hat{a}$, $\hat{a}^\dagger$, $\hat{M}$, $\hat{M}^\dagger$, $\hat{N}_a$, and $\hat{N}_b$ can simply be replaced by the c-number variables $\mathcal{A}$, $\mathcal{A}^*$, $\mathcal{M}$, $\mathcal{M}^*$, $\mathcal{N}_a$, and $\mathcal{N}_b$, respectively, without formally changing the equations. The Monte Carlo integration consists of the following steps. First, one simulates the initial distribution function by a statistical ensemble of the system variables. An element of the ensemble is a randomly chosen $\{\mathcal{A}(0),\mathcal{A}^*(0),\mathcal{M}(0),\mathcal{M}^*(0),\mathcal{N}_a(0),\mathcal{N}_b(0)\}$ set. From each initial condition set, a given "history" is derived by numerically integrating Eqs. (1). At any time t, a statistical ensemble of c-number sets $\{\mathcal{A}(t),\mathcal{A}^*(t),\mathcal{M}(t),\mathcal{M}^*(t),\mathcal{N}_a(t),\mathcal{N}_b(t)\}$ represents the system variables. The quantum-mechanical average of any physical quantity which depends on the system variables is obtained by averaging the corresponding c-number expression over the statistical ensemble defined by the initial distribution function.

The c-number functions $\mathcal{F}$ corresponding to the Langevin noise operators should be considered stochastic variables, with zero averages. Their correlation functions can be expressed in terms of redefined diffusion coefficients, obtained from Eqs. (3) and from the conditions that the c-number equations should yield the same second-order moments as the operator equations, for the previously defined ordering [17]. The resulting theory is reliable as long as at most second-order correlations are concerned. Even though one should expect this condition to be valid in the high-intensity region, its validity is not guaranteed around threshold. We will show nevertheless that the numerical and the analytical solutions agree very well over a wide region of laser operation, which may go from below threshold to high above it.

As a consequence of our stochastic c-number representation of the Langevin forces, each "history" of the system variables becomes *de facto* stochastic. We are thus dealing with a "double Monte Carlo method," generating an ensemble of random trajectories from randomly selected initial conditions.

We use the symmetric operator ordering for which the corresponding distribution function (Wigner function) is always real. For this ordering, the diffusion coefficients of the c-number Langevin forces can be written

$$2\mathcal{D}_{ij} = D_{ij} + D_{ji}, \tag{60}$$

where the c-number replacement must be performed on the right-hand side in D_{ij} and D_{ji} [all nonvanishing coefficients are given in Eqs. (3)]. One should note that the diffusion coefficients depend on the system variables. It is easy to check, for the system considered here, that the diffusion coefficients will be always positive, which is an essential condition for the applicability of the method.

B. Implementation

Having given the basic principles of our numerical method, we now consider the details of the computation. The problem consists in integrating a set of coupled nonlinear stochastic differential equations. For each step (duration dt), one should account for two kinds of contributions. The first one is the deterministic evolution due to the atom-light interaction, simply treated by a Runge-Kutta step. The second is the Brownian motion due to the random effect of the large reservoir on the small quantum systems. The accumulated action of a δ-correlated random force in a dt interval yields a random displacement that follows Gaussian statistics with a variance proportional to dt. Therefore, the diffusion coefficients in Eqs. (60) are multiplied by dt to yield the variances for the Gaussian random variables. One must then generate six random numbers obeying the correlation and cross-correlation relations given by Eqs. (60). The cross-correlations for the atomic random displacements can be taken into account by a linear transformation on four inde-

pendent Gaussian stochastic variables. This operation requires the diagonalization of a 4×4 diffusion matrix in each step.

We note here that, when using normal ordering, the diffusion matrix could have negative eigenvalues. Even though this fact does not prevent getting correct results for the physically relevant quantities [17,18], it makes it impossible to simulate the evolution with Gaussian random variables. This explains why we have chosen here the symmetrical ordering, which yields always positive diffusion coefficients.

The correlations depend on reservoir-averaged values of the system variables. For the system evolution from t to $t + dt$, one needs to know these averages. To this end, the histories must be simulated in parallel, which puts severe requirements on the computer memory but not on the simulation time.

In conclusion, we have developed a method that enables us to simulate numerically the dynamics of a damped quantum system. Our approach, which allows the treatment of a set of equations describing the laser in the nonlinear regime, has two limitations: the loss of precision due to statistical effects of the Monte Carlo method, and the fact that we do not treat correlations of the field and atomic variables at orders higher than the second. In spite of this, the agreement with the analytical solutions is very good. The computational effort is minimum: only two complex (field amplitude, atomic polarization) and two real (atomic populations) quantities are calculated (although many times for establishing a good statistics). At variance, the Schrödinger-Markov approach leads to an enormous number of variables when the photon number is large. Our method, based on the Heisenberg-Langevin picture, applies for the usual lasers as well as for microlasers.

VI. COMPARISON OF THE MODELS

The remaining part of this paper will be devoted to a comparison of the results of the models introduced above, i.e., the rate-equations model, the approximate quantum model, and the numerical model. They will also be compared to the very simple Lamb model. We will then use these models to make quantitative predictions for a thresholdless microsphere laser, under construction.

A. Semiclassical limit

In this subsection we analyze the behavior of the various models in the semiclassical regime, achieved at very high pumping rates and resulting in an intense field in the cavity mode. Intuitively, it is expected that all models should converge toward the Lamb one.

We show first that the approximate quantum model, though it is expected to be valid only near threshold, gives a steady-state average number of photons very close to the Lamb result I_0. Expanding the steady-state solution (53) in terms of $r \gg 1$, we obtain the dominant terms

$$i_{\mathrm{qm}} = r - 1 + c\Gamma_a / \Gamma_b + O(1/r). \qquad (61)$$

The asymptotic photon number mismatch with the Lamb model, $I - I_0$, is given by

$$I_{\mathrm{qm}} - I_0 \rightarrow \frac{1}{1 + \kappa/2\Gamma_{ab}} \frac{\Gamma_a/\Gamma_b}{1 + \Gamma_a/\Gamma_b}. \qquad (62)$$

This quantity is always smaller than Γ_a/Γ_b, much lower than 1 for any practical laser situation. Therefore, there is a negligible difference between the quantum and Lamb model results as expected in the semiclassical high-intensity regime [17].

Let us now expand the steady-state intensity (20), obtained from the rate-equation model (13), into powers of the normalized pumping rate:

$$i_{\mathrm{re}} = r - 1 - \frac{\kappa/2}{\Gamma_{ab}} + \frac{2g^2}{\Gamma_{ab}\Gamma_b} + O(1/r). \qquad (63)$$

The intensity difference with the Lamb model can be expressed, in terms of photons number, in the $r \rightarrow \infty$ limit, as

$$I_{\mathrm{re}} - I_0 \rightarrow -\frac{\Gamma_a\Gamma_b\kappa}{4g^2(\Gamma_a + \Gamma_b)} + \frac{\Gamma_a}{\Gamma_a + \Gamma_b} \approx \frac{\kappa\Gamma_a}{4g^2}. \qquad (64)$$

This mismatch, which increases with the cavity damping rate κ, may be large for realistic parameters. Moreover, the intensity is predicted to be lower than I_0, yielding an inversion higher than the Lamb's model inversion:

$$\Delta_{\mathrm{re}} - \Delta_0 \approx \frac{\kappa^2}{4g^2}, \qquad (65)$$

a quite intriguing result. Our quantum model predicts that a solution with such a population inversion should be unstable. It would be interesting to check whether the full Heisenberg-Langevin equations, linearized around the operating point predicted by the rate-equation approach (linearization is possible in the semiclassical regime), predict a stable or unstable solution. This work is under progress. In the following we will find other indications of a failure of the rate-equation model in the high-intensity limit, particularly in the bad-cavity case.

B. Characterization of thresholdless behavior

Expression (53) can be used to give a very natural definition of the thresholdless laser regime. Many definitions of the laser threshold in such regimes have already been proposed. The one we discuss here relies only on the input-output characteristic of the laser, which can be easily measured experimentally. In the semiclassical regime, $I(R)$ response presents a slope discontinuity at threshold. For a laser operating near the thresholdless regime, this discontinuity disappears. One might expect that the $I(R)$ curve becomes smoother and smoother when the laser approaches thresholdless operation. It thus seems natural to define the threshold as the point where the second derivative of the intensity with respect to the pumping rate is at a maximum, and to characterize the "distance" to the thresholdless regime by the maximum value of the curvature. A closely related definition based on second-order intensity correlation functions was proposed in Ref. [27]. In Lamb's semiclassical theory, this definition of the threshold obviously coincides with the standard one. The second derivative turns out to

have, in our approximate quantum model, a maximum at the normalized pumping rate $r_{qm, th}$ given by

$$r_{qm, th} = 1 - c(1 + 2\Gamma_a/\Gamma_b). \qquad (66)$$

When the parameter c is much lower than 1, this yields $r = 1$, in agreement with the Lamb model. When c increases, the threshold decreases and the thresholdless laser condition reads as

$$\frac{W}{\Gamma_a}\left(1 + \frac{2\Gamma_a}{\Gamma_b}\right) > 1. \qquad (67)$$

If $\Gamma_a \ll \Gamma_b$, we simply obtain

$$c = \frac{W}{\Gamma_a} > 1. \qquad (68)$$

The parameter c represents the ratio of W, the rate of spontaneous emission into the laser mode to the total relaxation rate of level a. It measures the spontaneous emission efficiency from level a into the cavity mode as compared to other decay processes. As stated earlier, the connection between c and β depends on the characteristics of the dipole and of the cavity under consideration, and it is not always sufficient to reach the limit $\beta \rightarrow 1$ to observe thresholdless lasing. In fact, when Eq. (17) applies, one has

$$\beta = \frac{c}{c + \Gamma_a^{sp}/\Gamma_a}, \qquad (69)$$

which yields a simple relation between the parameters β and c, when spontaneous emission is the only source of decay of the population from level a ($\Gamma_a^{sp} = \Gamma_a$). One then has $\beta = c/(1+c)$. In this case, the extreme thresholdless limit $c \gg 1$ corresponds to $\beta \rightarrow 1$, while $\beta \rightarrow 0$ is associated with a regime reminiscent of the semiclassical threshold. One should note, however, that there could be a well-marked threshold even if $\beta \sim 1$, as long as other decay channels are available and $\Gamma_a^{sp} \ll \Gamma_a^*$. Note also that, from Eq. (51), $c \approx I_{sat}^{-1}$ if $\kappa \lesssim \Gamma_{ab}$ (good cavity) and $\Gamma_a \lesssim \Gamma_b$. Thus, in this case, the criterion for thresholdless lasing is $c \approx I_{sat} \sim 1$. On the other hand, if $\kappa \gg \Gamma_{ab}$ (bad-cavity limit), the thresholdless behavior implies $I_{sat} \ll 1$.

When the thresholdless condition is not met, the "distance" from the thresholdless regime can be characterized by the value of the curvature at threshold.

$$\eta \equiv \left(\frac{\partial^2 i}{\partial r^2}\right)_{r_{qm, th}} = \frac{1}{4}\left[\left(1 + \frac{\Gamma_a}{\Gamma_b}\right)c\left(1 - \frac{\Gamma_a}{\Gamma_b}c\right)\right]^{-1/2}. \qquad (70)$$

If $\Gamma_a \ll \Gamma_b$, then this expression reduces to

$$\eta = \frac{1}{4}\frac{1}{\sqrt{c}}. \qquad (71)$$

In Fig. 2 we represent normalized intensity $i_{qm} = I/I_{sat}$ curves as a function of the normalized pumping rate $r = R/R_{th}$ for various parameters c. The progressive evolution from the semiclassical regime, where there is a discontinuity of the slope, to the thresholdless laser, where the curvature of
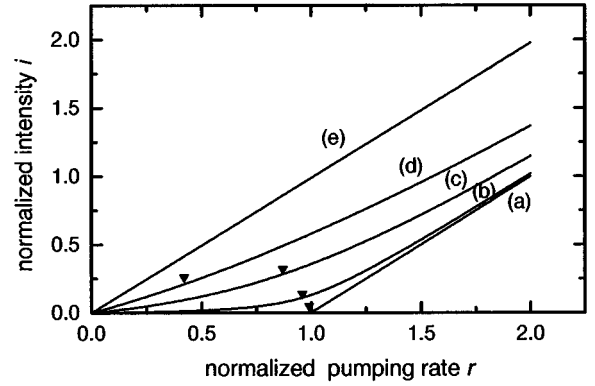

FIG. 2. Normalized intensity $i = I/I_{sat}$ vs normalized pumping rate $r = R/R_{th}$. The parameter c is chosen to be 0.0008, and 0.02, 0.2, 0.8, 80, for curves (a), (b), (c), (d), and (e), respectively. For the smaller c values, the semiclassical threshold is clearly apparent. Small arrows indicate the positions of threshold defined as the position of the maximum curvature. When c increases, the threshold comes closer to zero pumping, until it finally disappears for $c \simeq 1$.

the $I(R)$ curve decreases montonically, is apparent. The arrows indicate, for each curve, the position of the threshold defined as above.

Let us note that the rate equations lead, with the previous definition of the laser threshold, to the same condition (67) for a thresholdless laser. On the other hand, when there is a clearly defined threshold, the corresponding pumping rate differs from the one given in Eq. (66). In terms of pumping rates, we immediately obtain

$$R_{re, th} = R_{qm, th}\frac{\Gamma_{ab} + \kappa/2}{\Gamma_{ab}}. \qquad (72)$$

Even in the semiclassical regime, where all models should converge to the Lamb one, rate equations (13) may predict a threshold different from the usual one. The difference is vanishingly small in the good-cavity limit, when Γ_{ab} is by far the highest damping rate, and the adiabatic rate equations (14) apply. For bad cavities, the difference is large. Moreover, in the very bad-cavity limit, the above equation predicts a quadratic variation of the threshold with the cavity damping rate. This is at complete variance with the expectations for a semiclassical laser. This result seems to indicate that the rate equations (13) correctly describe the laser only in the good-cavity limit. Since the only approximation leading to these equations is the decorrelation hypothesis, this shows that the quantum correlations between the atomic inversion and the photon number play an important role for the evolution of the quantum averages. This can be understood qualitatively. When the laser intensity increases, the absolute amplitude of the photon number fluctuations increases, roughly as the square root of the laser intensity. Since the average population inversion is clamped, the relative fluctuations of the populations are increasing with the intensity. The correlation between these quantities may therefore play an increasing role in the laser dynamics. This is of course only a qualitative argument. It is somewhat supported by the numerical simulations, where the correlations can be estimated. They effectively play an increasing role at high intensity and

contribute by an increase of the laser intensity and a diminution of the population inversion. A much more detailed analysis of these correlations is in high demand to clarify this point.

C. Application of the models to the microsphere laser

We discuss now the results from the above models. To clarify the discussion and make it relevant to the experiments in progress, we will restrict the parameter space to the one of the Nd microsphere laser described in Ref. [7]. Let us stress that our quantum model is not restricted to the study of this very peculiar laser, and could be adapted to very many other situations.

1. Parameters relevant to the microsphere laser

The system considered in Ref. [7] was a multimode laser. The total linewidth of the neodymium transition (about 60 nm) includes the nonresolved contributions of many inhomogeneously broadened transitions between various sublevels. It was much larger than the spacing between adjacent modes of the microspherical resonator (about 4.5 nm). However, this mode spacing is at least comparable with the homogeneous linewidth of the ionic transition (1500 GHz at room temperature, corresponding to about 5 nm, of the same order of magnitude as the inhomogeneous broadening for a single transition). The ions whose frequency is within one homogeneous linewidth from a resonant mode of the microsphere have only a slight interaction with the other modes. Independent cavity modes therefore interact with independent ionic populations. Furthermore, it was observed in the experiment [7] that all the lasing modes have approximately the same threshold. It is thus a good approximation to ignore the multimode nature of the radiated field, replacing it by an effective interaction between the atoms and a single mode of the field. The corresponding coupling constant, which mimics the couplings and frequencies of the different atoms, is an adjustable parameter, which can be determined from the experimental data.

For the upper state of the lasing transition, Γ_a has been measured to be $\Gamma_a = 1$ krad/s. The relaxation rate of b is much higher. Since it does not enter in the final results as long as it is much larger than Γ_a, it can be taken as $\Gamma_b = 10$ Mrad/s. The cavity damping rate κ is, for the best spheres, of the order $\kappa = 10$ Mrad/s. It can be increased at will by adjusting the distance between the sphere and the coupling prism used to feed in the pumping light [7]. The coupling parameter g is not very well known experimentally, since it depends on the sphere mode volume which cannot be determined directly. In this discussion we will use two different values, $g = 0.1$ and 1 Mrad/s, which should span the entire variation range.

Finally, the homogeneous linewidth Γ_{ab} is close to 5000 Grad/s at room temperature. When the sphere temperature is reduced, this relaxation rate is bound to decrease, due to the lowering density of phonons in the material. Though this temperature dependence is not very well known experimentally, one might expect $\Gamma_{ab}(T) \sim T^2$ down to quite low temperatures. Therefore, taking $\Gamma_{ab}(T = 300$ K$) = 5000$ Grad/s as a reference, we may approximate $\Gamma_{ab}(T) \approx 50T^2$ Mrad/s, where the temperature is given in

Kelvin. At very low temperature, this behavior is bound to saturate, and we have used the minimum value $\Gamma_{ab}(T = 0$ K$) = 20$ Mrad/s (the actual value is yet completely unknown experimentally). With this range of variation of Γ_{ab} and κ, the laser can operate either in an ordinary semiclassical regime, with a well-marked threshold, or in a thresholdless one.

2. Average number of photons and population inversion

The intensity of the laser mode is plotted against the pumping rate in Fig. 3. For Figs. 3(a) and 3(b), the cavity relaxation rate κ is chosen to be 10 Mrad/s, and the coupling parameter is set to $g = 1$ and 0.1, respectively. The threshold disappears and a deviation from the semiclassical theory can be observed in a wide range of the pumping rate, even far from the semiclassical threshold. The approximate analytical model [Eq. (53)] is in excellent agreement with the numerical results in both cases. As expected from the general discussion, it can be seen in Fig. 3(b) that the rate equations predict a somewhat smaller operating intensity. This behavior is more conspicuous in Fig. 3(c), where the cavity has a high relaxation rate ($\kappa = 100$ Mrad/s,$g = 0.1$ Mrad/s). It is quite apparent from this figure that the threshold predicted by the rate equations, by extrapolation of the linear asymptotic behavior, is significantly different from the Lamb one.

To make this mismatch more evident, in Fig. 4 we plot the analytical and numerical results for the population inversion (in number of atoms) versus the pumping rate. The analytical curves are derived from Eqs. (20) and (53) with the help of the balance equation (12). Any mismatch between the different models for the steady-state intensities is amplified by a factor $\Delta_0 / I_{sat} = \kappa(\Gamma_a + \Gamma_b)/\Gamma_a\Gamma_b \approx \kappa/\Gamma_a$ for the population inversion. This factor is of the order of 10^4 for the explored range of the parameters. The population inversion is therefore much more sensitive to the validity of the models than the intensity. The results provided by the two analytical approaches are in good agreement in the region near and below the semiclassical threshold [see the inset in Fig. 4(a) for $g = 1$ Mrad/s and $\kappa = 10$ Mrad/s]. They start to deviate in an intermediate pumping regime between the threshold and the inversion clamping region, while the analytical quantum model's curve still fits well on the numerical data. Finally, for high pumping, the inversion is clamped at different values, as already discussed in Sec. VI A. Within the numerical precision, in this high pumping regime, the numerical results tend towards the semiclassical one, Δ_0, without any remaining mismatch. In accordance with the original assumption expressed in Eq. (29), i.e., a population inversion much larger than the photon number in the mode, the approximate quantum model's agreement with the numerical values is slightly worse for higher pumping. However, the maximum difference does not exceed 5%. Although the validity of the quantum model approximation can be questioned for such pumping rates, it seems to reproduce the numerical predictions satisfactorily.

On the other hand, as shown in Fig. 4(c), in the case of a bad cavity ($g = 1$ Mrad/s,$\kappa = 100$ Mrad/s) the rate equations yield a population inversion strikingly different from the ones, more or less equal, predicted by the three other models.
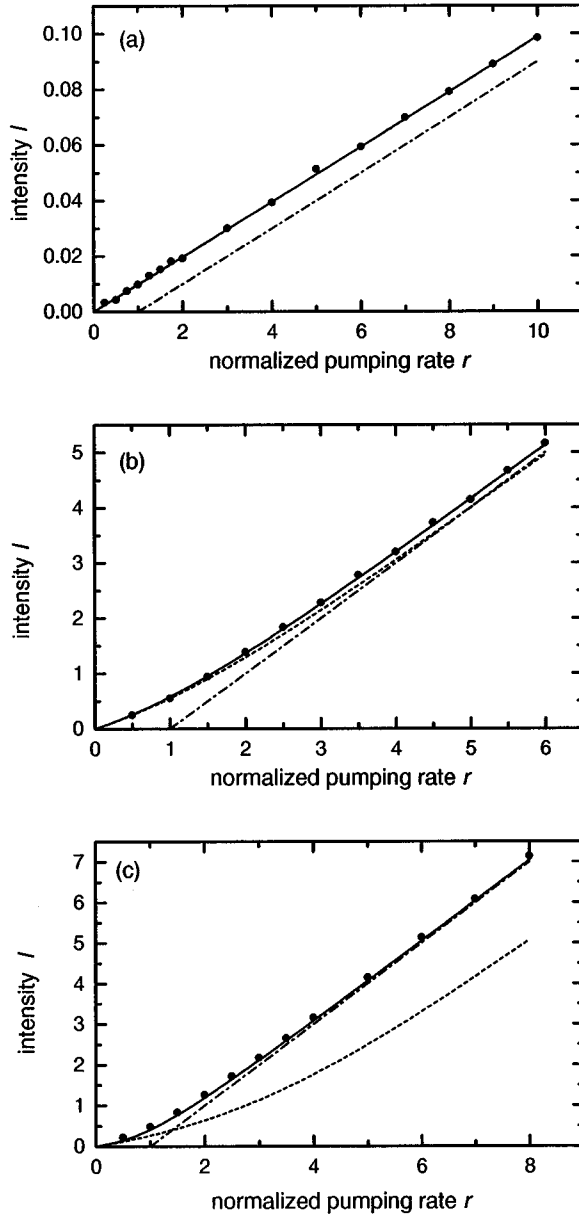
FIG. 3. Mean photon number I vs normalized pumping rate r found numerically (solid dots), analytically from the quantum model (solid line) or analytically from the rate equations (short dashed line). The semiclassical linear dependence is displayed (dotted-dashed line) as well. Values of the parameters (in Mrad/s) are $\Gamma_b = 10$, $\Gamma_a = 0.001$, and $\Gamma_{ab} = 20$. To explore a wide range of different output characteristics, g and κ are varied: (a) $g = 1$ Mrad/s, $\kappa = 10$ Mrad/s; (b) $g = 0.1$ Mrad/s, $\kappa = 10$ Mrad/s; and (c) $g = 0.1$ Mrad/s, $\kappa = 100$ Mrad/s. These parameter sets correspond to operating points (a) $c = 80$ (far in the thresholdless regime), (b) $c = 0.8$ (almost a thresholdless laser), and (c) $c = 0.27$ (weak threshold).

3. Spectrum

Figure 5 compare the phase diffusion linewidth $2|\lambda_-|$ as a function of the pumping rate, obtained from Eq. (57), with the numerical results. Analytical and numerical results are very close to each other. These figures show clearly that the quantum model may safely be used to determine the laser spectrum. Some estimate of the linewidth can be inferred
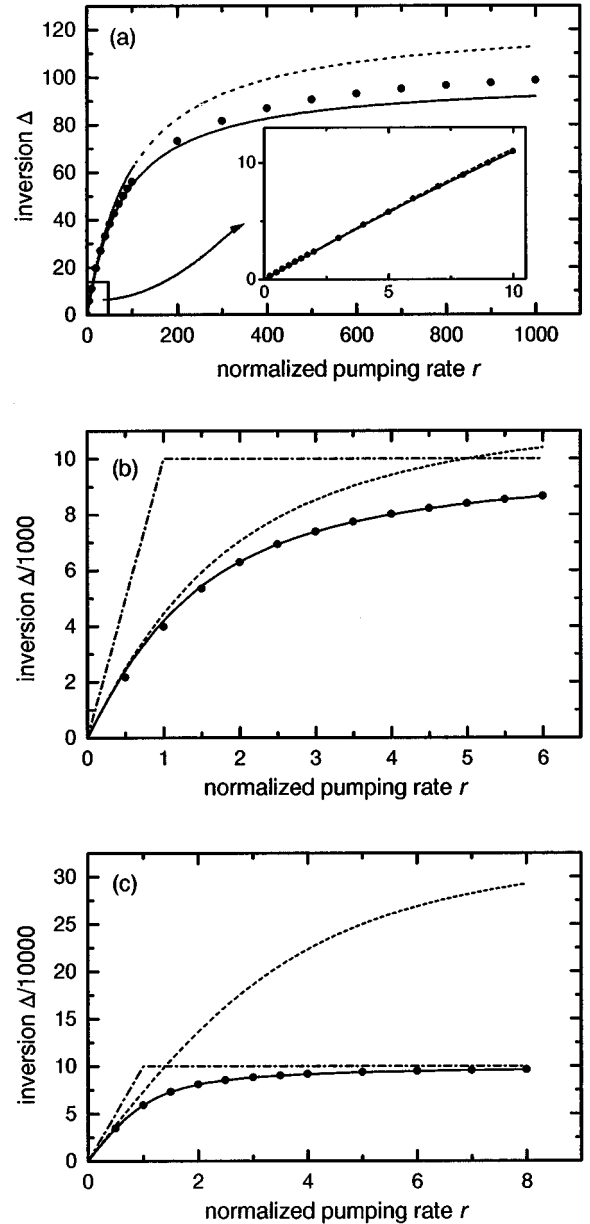
FIG. 4. Steady-state population inversion Δ vs normalized pumping rate r, calculated numerically (solid dots) and analytically from the quantum model (solid line) and the rate equations (short dashed line). The semiclassical clamped inversion is shown by the dotted-dashed line. Parameter values are the same as for Figs. 3(a), 3(b), and 3(c), respectively. In the inset of (a), a pumping rate range corresponding to Fig. 3(a) is plotted.

from the rate-equation approach as well. The eigenfrequencies of the rate-equation system, linearized around its steady-state operating point, should give an indication of the linewidth, as in the quantum approach.

For the case $g = 1$ Mrad/s and $\kappa = 10$ Mrad/s represented in Fig. 5(a), there are two distinct, real eigenvalues below a well-defined pumping rate. Above this pumping rate, corresponding to the singular point in Fig. 5(a), the two eigenvalues become complex (above this point, we plot only the real part of the eigenvalues). A complex eigenvalue means that the laser undergoes relaxation oscillations, not found in the quantum model. We note that one of the eigenfrequencies of
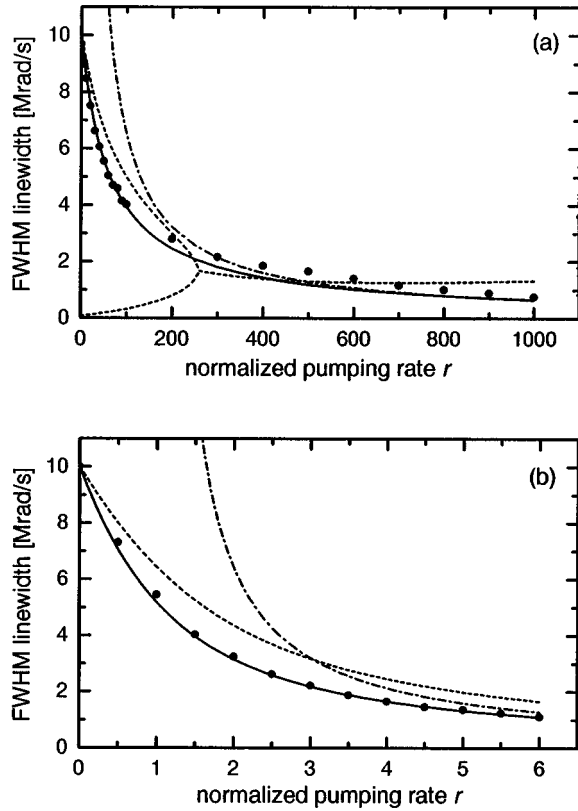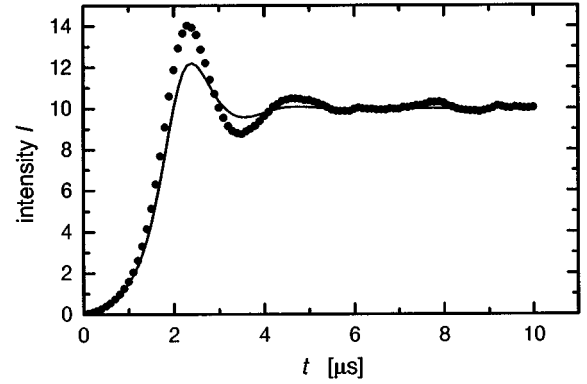
FIG. 6. Transient behavior of the laser intensity. The solid curve found is from quantum theory, the dashed curve from the rate-equation model. Parameters are the same as for Fig. 3(a), and the pumping rate is $r=1000$ in terms of threshold pumping rate. For the same parameter setting, the semiclassical theory predicts much more accentuated oscillations, attaining a maximum photon number of about 50.

FIG. 5. Laser linewidth found numerically (solid dots) and analytically from the quantum model (solid line) for the parameter values (in Mrad/s) $\Gamma_a=0.001$, $\Gamma_b=10$, and $\Gamma_{ab}=20$. (a) and (b) correspond to $g=1$ Mrad/s, $\kappa=10$ Mrad/s and $g=0.1$ Mrad/s, $\kappa=10$ Mrad/s, respectively. The short dashed lines represent two eigenfrequencies of the rate equations linearized around the steady state. In (a), the two eigenfrequencies become degenerate at a certain pumping rate. Above this pumping rate, they have nonvanishing imaginary parts indicating the presence of relaxation oscillations. The dash-dotted line represents a Schawlow-Townes law adjusted to the high-above-threshold regime.

the rate-equation model approaches quite well, at least qualitatively, the numerically calculated linewidths. For the other parameter settings, $g=0.1$ Mrad/s and $\kappa=10$, there is no complex eigenvalue within the plotted range of pumping rate [Fig. 5(b)].

The analytical solution for the linewidth in Eq. (57), in the high pumping regime, leads to a modified Schawlow-Townes limit. Approximation (59) pertains to this case. The difference $i_{qm}-i_0$ can be expressed by means of expanding solution (53) into powers of $1/i_0$. Thus one obtains

$$2|\lambda_-| \cong \frac{\kappa\Gamma_{ab}}{\kappa/2+\Gamma_{ab}}\frac{c}{i_0}\left[1+(1+i_0-c)\frac{\Gamma_a}{\Gamma_b}-c\left(\frac{\Gamma_a}{\Gamma_b}\right)^2\right]$$
$$+O(1/i_0^2). \tag{73}$$

The Schawlow-Townes formula is recovered in the limit $\Gamma_a/\Gamma_b\to0$,

$$2|\lambda_-| \cong \frac{\kappa\Gamma_{ab}^2}{(\Gamma_{ab}+\kappa/2)^2}\frac{1}{I_0}, \tag{74}$$

reducing to κ/I_0 in the good-cavity limit, as expected. Otherwise, the linewidth tends to a finite value when $i_0\gg1$. With our parameter setting, Γ_a/Γ_b is negligible. As a result, the Schawlow-Townes law, properly scaled, fits quite well with the laser linewidth (see Fig. 5).

The quantum-mechanical model never exhibits relaxation oscillations in the laser intensity. They are clearly ruled out by the assumption that the population inversion is nearly a constant. Since the rate-equation model predicts such oscillations for a high enough pumping rate, it is interesting to look at the numerical predictions. We display the transient buildup of the laser field at pumping rate $r=1000$ in Fig. 6, and compare the numerical results with the predictions of the quantum and rate-equation models. One observes effectively small-amplitude oscillations, not predicted by the quantum model. Note that the relaxation oscillations predicted by the Lamb semiclassical model have a much larger amplitude, equal to five times the steady-state intensity. The rate equations (13), which fail to describe correctly the lasers far above threshold, nevertheless correctly predict these oscillations. Since the relaxation oscillations are easily observable experimentally, it would be extremely interesting to study them in detail in order to check the validity of the models.

VII. CONCLUSIONS

In this work we have presented a theoretical analysis of a thresholdless laser. We have solved the problem by two different procedures: an analytical quantum model, based on neglecting the fluctuations in the atomic inversion; and a numerical integration of the corresponding nonlinear stochastic Langevin equations. We have also compared the predictions of these models to the ones of a rate-equation approach, which takes into account spontaneous emission and does not require the adiabatic elimination of the polarization. The numerical predictions and the quantum model agree quite well, either for the laser intensity or for more subtle quantities such as the laser spectrum, in a very wide range of parameters. Moreover, these two models nicely converge toward the Lamb semiclassical predictions at high intensity.

The agreement with the quantum rate equations is less impressive, especially at high intensities. These results cast some doubt on the rate-equation model, particularly in the bad-cavity limit.

We use also the quantum model to shed some light on the role of the spontaneous emission rate in the laser cavity. We give a definition of the laser threshold and of the thresholdless laser regime which can be easily used experimentally, since it is based only on the intensity vs pumping characteristic of the laser. The thresholdless regime is defined by a simple and intuitive criterion: the spontaneous emission rate in the mode should dominate the decay rate of the upper level of the lasing transition. When the only decay channel from level a is spontaneous emission into the lasing mode, thresholdless operation occurs as soon as $\beta \simeq 1$. When level a may decay by nonradiative channels, we show that this definition does not hold any longer. The laser might still have a well-marked threshold in spite of a large β factor.

Finally, we have studied in detail the models in the case of neodymium-doped microsphere lasers. We have shown that the thresholdless regime could be reached experimentally at low temperatures. We have also calculated the power spectrum of the laser field, obtaining an expression which can be applied to the region close to threshold, when both phase diffusion and photon-number fluctuations contribute to the linewidth, and which reproduces the well-known Schawlow-Townes spectrum when the laser is well above threshold. The experiment aiming at testing these results on a microsphere laser are now under progress.

ACKNOWLEDGMENTS

APPENDIX: INTEGRAL IN EQ. (47)

In this appendix we calculate the integral

$$J = \frac{1}{2\pi} \int \frac{d\omega}{|D(\omega)|^2} \qquad (A1)$$

where, according to Eq. (41),

$$|D(\omega)|^2 = (\omega^2 + \lambda_+^2)(\omega^2 + \lambda_-^2),$$

with

$$\lambda_+^2 + \lambda_-^2 = -2g^2(\Delta_0 - \Delta) + \left(\frac{\kappa}{2} + \Gamma_{ab}\right)^2,$$

$$\lambda_+^2 \lambda_-^2 = g^4(\Delta_0 - \Delta)^2. \qquad (A2)$$

The integral J can be performed by going through the following steps:

$$
\begin{aligned}
J &= \frac{1}{2\pi} \int \frac{d\omega}{(\omega^2 + \lambda_+^2)(\omega^2 + \lambda_-^2)} \\
&= \frac{1}{2\pi} \frac{1}{\lambda_-^2 - \lambda_+^2} \int \left[\frac{1}{\omega^2 + \lambda_+^2} - \frac{1}{\omega^2 + \lambda_-^2} \right] d\omega \\
&= \frac{1}{2\pi} \frac{1}{\lambda_-^2 - \lambda_+^2} \left[\frac{1}{|\lambda_+|} - \frac{1}{|\lambda_-|} \right] \int \frac{dy}{1 + y^2} \\
&= \frac{1}{2} \frac{|\lambda_-| - |\lambda_+|}{|\lambda_-||\lambda_+|(\lambda_- + \lambda_+)(\lambda_- - \lambda_+)} \\
&= \frac{1}{2} \frac{1}{|\lambda_-||\lambda_+|(|\lambda_-| + |\lambda_+|)},
\end{aligned}
$$

where we obtain from Eq. (A2) that

$$|\lambda_+||\lambda_-| = g^2|\Delta_0 - \Delta|,$$

$$(|\lambda_+| + |\lambda_-|)^2 = \lambda_+^2 + \lambda_-^2 + 2|\lambda_+||\lambda_-|.$$

Since we know that $\Delta_0 > \Delta$, because of the stability of the solution, we can get rid of the absolute value signs and finally obtain

$$J = \frac{1}{2g^2(\Delta_0 - \Delta)(\kappa/2 + \Gamma_{ab})}. \qquad (A3)$$

[1] F. De Martini and G. R. Jacobovitz, Phys. Rev. Lett. **60**, 1711 (1988).

[2] F. S. Choa, M. H. Shih, J. Y. Fan, G. J. Simonis, P.-L. Liu, T. Tanbun-Ek, R. A. Logan, W. T. Trang, and A. M. Sergent, Appl. Phys. Lett. **67**, 2777 (1995).

[3] D. L. Huffaker, J. Shin, and D. G. Deppe, Appl. Phys. Lett. **66**, 1723 (1995); D. L. Huffaker, H. Deng, Q. Deng, and D. G. Deppe, *ibid.* **69**, 3477 (1996).

[4] Z. Feit, M. McDonald, R. J. Woods, V. Archambault, and P. Mak, Appl. Phys. Lett. **68**, 738 (1996).

[5] H. Taniguchi, H. Tomisawa, and J. Kido, Appl. Phys. Lett. **66**,

1578 (1995); S. Tanosaki, H. Taniguchi, K. Tsujita, and H. Inaba, *ibid.* **69**, 719 (1996).

[6] K. An, J. J. Childs, R. R. Dasari, and M. S. Feld, Phys. Rev. Lett. **73**, 3375 (1994).

[7] V. Sandoghdar, F. Treussart, J. Hare, V. Lefèvre-Seguin, J.-M. Raimond, and S. Haroche, Phys. Rev. A **54**, R1777 (1996).

[8] G. P. Agrawal and G. Gray, Appl. Phys. Lett. **59**, 399 (1992).

[9] G. Björk, A. Karlsson, and Y. Yamamoto, Appl. Phys. Lett. **60**, 304 (1992).

[10] G. Björk, A. Karlsson, and Y. Yamamoto, Phys. Rev. A **50**, 1675 (1994).

[11] T. Baba, T. Hamano, F. Koyama, and K. Iga, IEEE J. Quantum Electron. **27**, 1347 (1991); G. Björk, S. Machida, Y. Yamamoto, and K. Igeta, Phys. Rev. A **44**, 669 (1991).

[12] F. De Martini, G. Innocenti, G. R. Jacobovitz, and P. Mataloni, Phys. Rev. Lett. **59**, 2955 (1987).

[13] H. Haug, Phys. Rev. **184**, 338 (1969).

[14] G. M. Stéphan, Phys. Rev. A **55**, 1371 (1997).

[15] M. Asada, A. Kameyama, and Y. Suematsu, IEEE J. Quantum Electron. **QE-20**, 745 (1984).

[16] K. M. Gheri, D. F. Walls, and M. A. Marte, Phys. Rev. A **46**, 6002 (1992).

[17] L. Davidovich, Rev. Mod. Phys. **68**, 127 (1997).

[18] J. Bergou, L. Davidovich, M. Orszag, C. Benkert, M. Hillery, and M. O. Scully, Phys. Rev. A **40**, 5073 (1989); C. Benkert, M. O. Scully, J. Bergou, L. Davidovich, M. Hillery, and M. Orszag, *ibid.* **41**, 2756 (1990).

[19] H. J. Carmichael, Phys. Rev. A **33**, 3262 (1986); J. Y. Courtois, A. Smith, C. Fabre, and S. Reynaud, J. Mod. Opt. **38**, 177 (1991); M. I. Kolobov, L. Davidovich, E. Giacobino, and C. Fabre, Phys. Rev. A **47**, 1431 (1993).

[20] S. Prasad, Phys. Rev. A **46**, 1540 (1992).

[21] W. E. Lamb, Jr., Phys. Rev. **134**, 1429 (1964). Or, see, e.g., W. H. Louisell, *Quantum Statistical Properties of Radiation* (Wiley, New York, 1990); M. Sargent, III, M. O. Scully, and W. E. Lamb, Jr., *Laser Physics* (Addison-Wesley, Reading, MA, 1974).

[22] This is the case in Lamb's semiclassical treatment, where the field is consistently considered as a *c*-number, and spontaneous emission is therefore completely neglected. Other semiclassical approaches introduce spontaneous emission contributions by hand, as opposed to the first-principles derivation presented here.

[23] C. Cohen-Tannoudji, J. Dupont-Roc, and G. Grynberg, *Atom-Photon Interactions* (Wiley, New York, 1992). This textbook can be used to write the ratio between W and Γ_a^{sp} in a medium of index N if one considers that the dipole properties are not affected by the cavity boundaries. The relation between Γ_a^{sp} in a medium of index N and its counterpart in free space is a more delicate subject discussed, for instance, in P. W. Milonni, J. Mod. Opt. **42**, 1991 (1995).

[24] E. M. Purcell, Phys. Rev. **69**, 681 (1946).

[25] M. P. van Exter, G. Nienhuis, and J. P. Woerdman, Phys. Rev. A **54**, 3553 (1996).

[26] R. Loudon, M. Harris, T. J. Shepherd, and J. M. Vaughan, Phys. Rev. A **48**, 681 (1993).

[27] R. Jin, D. Boggavarapu, M. Sargent, III, P. Meystre, H. M. Gibbs, and G. Khitrova, Phys. Rev. A **49**, 4038 (1994).